Solar Energy 295 (2025) 113523

Contents lists available at ScienceDirect

Solar Energy

journal homepage: www.elsevier.com/locate/solener

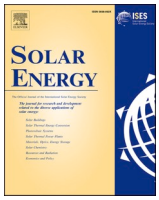

Driving forces of injection and regeneration in natural dye-sensitized solar cells: Insights into photovoltaic performance

M.E. Yelkovan [a,*], M. Erdogdu [b], Y. Erdogdu [c], A. Yildiz [a]

[a] Department of Energy Systems Engineering, Faculty of Engineering and Natural Sciences, Ankara Yildirim Beyazıt University, Ankara 06010, Turkey
[b] Department of Landscape Architects, Faculty of Agriculture, Kırşehir Ahi Evran University, Kırşehir 40100, Turkey
[c] Department of Physics, Faculty of Science, Gazi University, 06500 Teknikokullar, Ankara, Turkey

ARTICLE INFO

Keywords:
Hyoscyamus reticulatus
Mahonia aquifolium
Natural dye-sensitized solar cells

ABSTRACT

Practical fabrication, low costs, and environment-friendly energy harvesting are the most significant features of solar cells sensitized by natural dyes. However, the employment of natural dye reduces the cost of production while causing severe photovoltaic losses associated with magnitude of underlying forces behind electron injection and dye regeneration. Therefore, lack of knowledge based on these forces have limited the development of DSSCs. To overcome these obstacles for unveiling the performance DSSCs, herein, properties of DSSCs obtained from *Hyoscyamus reticulatus* (*HR*), and *Mahonia aquifolium* (*MA*) were comprehensively investigated. The magnitude of underlying forces behind electron injection (dye regeneration) was estimated to be 0.831 V (0.092 V) and 0.823 V (0.105 V) for *HR* and *MA*, respectively. These values were correlated with photovoltaic parameters. We noticed that driving force should be higher for electron injection while it should be lower for dye regeneration. Under standard AM 1.5G simulated solar radiation, *HR* based device shows a solar to electricity efficiency of 1.20 % (Fill factor of $FF = 0.67$; short-circuit current density of $J_{sc} = 2.66$ mA/cm^2; open circuit voltage of $V_{oc} = 0.67$ V) while *MA* based device shows an efficiency of 0.22 % ($FF = 0.37$; $J_{sc} = 1.34$ mA/cm^2; $V_{oc} = 0.45$ V).

1. Introduction

Dye-sensitized solar cells (DSSCs) have gained significant attention due to their cost-effectiveness, tunable optical properties, and potential for high efficiency. As global energy consumption hit 604.04 EJ in 2022, solar energy-especially DSSCs with natural dyes-gained attention for their design flexibility and potential to offset emissions, despite challenges in efficiency and stability [1]. The performance of DSSCs is primarily governed by their molecular sensitizers, which play three critical roles: (1) generating charge carriers upon photoexcitation, (2) facilitating electron injection into the conduction band, and (3) enhancing light absorption across the solar spectrum. Recent advances in counter electrode materials demonstrate that opaque Pt films exhibit superior reflectivity and electrocatalytic activity compared to transparent Pt, achieving a 5.06 % power conversion efficiency (PCE) due to reduced charge-transfer resistance and enhanced mechanical stability [2]. Alternatively, carbon-based CEs synthesized via low-temperature methods show promise, with homemade carbon paste achieving a 2.70 % PCE-1.6 fold higher than commercial carbon paste-owing to its porous structure and improved electrolyte diffusion [3]. Carbon-coated nanotextured silicon wafers used as counter electrodes in DSSCs achieved a power conversion efficiency of 6.73 %, demonstrating potential as a low-cost alternative to platinum-based electrodes [4]. For photoanodes, Ni-doped TiO_2 homojunction bilayers significantly enhance light absorption and electron transport, yielding a 6.08 % PCE by optimizing band alignment and reducing recombination [5]. Similarly, hybrid TiO_2 nanoparticle-nanorod photoanodes with a $TiCl_4$ blocking layer reach 5.58 % PCE, addressing interfacial connection issues [6], while hierarchical blocking layers boost efficiency by 40 % via suppressed charge recombination [7]. Recent advancements in DSSCs have demonstrated significant progress through innovative material engineering and natural dye optimization. Plasmonic enhancement via silver nanoparticle incorporation in TiO_2 photoanodes has proven particularly effective, with co-deposited Ag-TiO_2 configurations achieving a 94 % efficiency improvement (1.28 % PCE) due to enhanced light absorption and reduced charge recombination [8]. Natural dye exploration has expanded to novel sources like tender coconut husk, where solvent/extraction method optimization yielded PCEs up to 0.46 % [9], while

* Corresponding author.
E-mail address: meyelkovan@aybu.edu.tr (M.E. Yelkovan).

https://doi.org/10.1016/j.solener.2025.113523
Received 20 February 2025; Received in revised form 9 April 2025; Accepted 14 April 2025
Available online 21 April 2025

eumelanin-based DSSCs achieved 0.42 % PCE after UV treatment despite challenges with recombination rates [10]. These developments align with the focus on eco-friendly materials and cost-effective processing, where copper-based electrolytes and interface engineering emerge as key strategies for competitiveness against thin-film photovoltaics [11]. Collectively, these studies highlight the multifaceted approaches-from plasmonic enhancement to natural dye refinement-being pursued to advance DSSC technology toward sustainable energy solutions. In dye sensitizers, natural dyes extracted from fruits like Cornus mas L. and Juniperus sabina achieve PCEs up to 0.98 % and 0.55 %, respectively, with acidic solvent extraction improving light harvesting [12,13]. Carminic acid from cochineal insects outperforms other natural dyes (1 % PCE) due to its broad absorption spectrum and strong TiO_2 anchorage [14]. Additives like 1-butyl-3-methylimidazolium iodide further enhance natural dye performance, increasing PCE by 56 % [15]. Synthetic dyes, such as AZO-based and BODIPY-based sensitizers, show limited PCEs (0.47 % and 0.34 %, respectively) but provide insights into molecular design via theoretical studies [16,17]. Collectively, these innovations highlight pathways to replace Pt-based components, optimize charge transport, and leverage natural dyes for sustainable DSSC development.

The following characteristics are typically present in a DSSC's power conversion efficiency: the highest occupied molecular orbital (HOMO) energy must be below the electrolyte's energy level in order to accept the electron from a redox electrolyte pair, and the lowest unoccupied molecular orbital (LUMO) should have energy greater than that of the TiO_2 conduction band [14,17]. Obtaining suitable sensitizers with the characteristics mentioned before is necessary to design DSSCs.

Currently, there are many attempts on the application of natural DSSCs. To employ DSSCs using natural dyes as sensitizers, anthocyanins, flavonoid, chlorophylls and other compounds which were taken from leaves, flowers, and fruits were examined [18–21]. More recently, Iman et al. [18] extracted olive leaf dyes and used them as sensitizers in DSSCs. They worked on the impact of different drying times. Their maximum efficiency value was 0.31 %. The same researchers also present a novel natural dye extracted from *Laurus nobilis L* [19]. The value of 0.23 % of power conversion efficiency was reported. Mahapatra et al [20] reported a work on natural dyes found from *Bixa orellana*, *Mallotus phillipensis* and *Basella alba*. *Bixa orellana* dye based cells demonstrated an efficiency of 0.67 %. A natural dye was created by Rajaramanan et al. [21] using *Mussaenda erythrophylla flowers*. The cell consisting of dye obtained in ethanol achieved an efficiency of 0.41 %.

Despite encouraging outcomes, most natural dyes perform far worse in DSSCs compared to specially designed organic dyes. The lack of research concentrating on the cause of their subpar photovoltaic performance makes the problem unsolved. Therefore, charge separation properties of DSSCs assembled with natural dyes should be studied methodically to gain a deeper comprehension of why one dye outperforms the other, which can result in even more optimization. For this purpose, an assessment of the underlying forces behind electron injection and dye regeneration and an attempt to directly link these parameters with solar device performance is required.

Hyoscyamus species can be found all over the world and are classified as medicinal plants in the Solanaceae family [22]. Tropane alkaloids, primarily hyoscyamine and scopolamine, are abundant in *Hyoscyamus* species. [23]. *Hyoscyamus* is represented by six species in Türkiye. *Hyoscyamus* reticulatus is a plant with purple flowers and feathery, deeply serrated leaves. Its flowers smell unpleasant, and its taste is bitter. [24]. Purple petals of the species were used in this study. The genus *Mahonia*, which is native to North America, is in the Berberidaceae family and has about 100 species [25]. *Mahonia aquifolium,* which is widely used as an ornamental plant in Türkiye, is a 1–2 m tall, evergreen plant in the form of an upright shrub [26]. Waxy blue-black fruits of the species were used in this study.

In this study, we scrutinize two natural dyes sensitized devices: *HR*, which is produced from *Hyoscyamus reticulatus*, and *MA*, which is extracted from *Mahonia aquifolium.* By examining optical and electrochemical characteristics as well as electron transfer kinetics in the NDSSCs, we examine these natural dyes performance in depth. Herein, we take a closer look at the two main driving forces that can have a remarkably impact on the effectiveness of charge separation, consequently, device performance. We consider how the underlying forces behind electron injection and dye regeneration mechanisms affect the performance of the devices.

2. Experimental

Berries and petals were subjected to a drying process at 50 °C for around a day. Subsequently, dehydrated specimen were pulverized into powder. In extraction procedure, 50 ml of methanol and ethanol for *HR* petals and *MA* berries with a mass of 2 g were utilized respectively. The extraction process was performed individually for each sample, employing a mixer for 24 h. A heating approach was employed at 40 °C during the extraction phase. On the following day, the extract underwent filtration. Specimen were preserved at 4 °C, which are shielded from light exposure until analysis.

This work employed extracts from the berries of *Mahonia aquifolium,* and the petals of *Hyoscyamus reticulatus* as a natural dye to function as a photosensitizer in synthesizing DSSCs. Specimens of botanical species, namely the petals of *Hyoscyamus reticulatus*, and the berries of *Mahonia aquifolium* were collected in Kırşehir, Türkiye. All botanical specimens acquired from natural dyes were preserved in an herbarium. Procedures for extracting the natural dyes utilized in this investigation are thoroughly detailed in our prior publications [13,15]. To prepare and characterize the NDSSCs, we totally followed the same experimental procedures and characterization techniques described in our previously published papers [13,15]. The active area of the fabricated devices is 0.27 cm^2.

The phenolic and anthocyanin components in the extract made from the most effective solvent were discovered in this investigation. Pure methanol, ethanol, and a mixture of methanol and water (80:20 v/v) were the best extraction solvents for phenolic and anthocyanin content. It has been determined that the main phenolic component of *Mahonia* berries is chlorogenic acid, whereas cyanidin-3-O-glucoside is the main anthocyanin molecule [27].

Extracts obtained from the petals of plants in the genus *Hyoscyamus* contain several chemicals, including carotenoids, flavonoids, phenolic acids, and tropane alkaloids. The carotenoids comprise the compounds Lycopene, β-Carotene, and Zeaxanthin, among others. The flavonoids comprise the compounds Kaempferol, Quercetin, Luteolin, Apigenin, and Rutin. The phenolic acids comprise Caffeic, Ferulic, p-coumaric, Salicylic and Rosmarinic acids, among others. Tropane alkaloids comprise Norhioscyamine, Scopolamine, and Hyoscyamine, among others. Hyoscyamus species are particularly rich in tropane alkaloids. The tropane alkaloids can be found in lower concentrations in petals than in leaves and seeds. But Flavonoids are prevalent in the petals of the plant. It may also contain carotenoid pigments that impart color to the petals [28,29].

3. Results and discussion

To unequivocally confirm the transfer of electrons to TiO_2 from the extracted pigments of the dyes, we investigated vibration modes via FT-IR spectroscopy analysis displayed in Fig. 1. Unlike the OH stretching vibration occurring at the high wavenumber region, the C═O stretching vibration mode usually appears at the low wavenumber region [30,31] as labelled in Fig. 1.

Thus, it is reasonable to assume that both dyes show C═O and O-H groups that are functional as marked in Fig. 1a. Peaks of *HR* dye observed at 3671, 3353, 3225, and 1739 cm^{-1} can be ascribed to these vibrations. In contrast, the peaks for *MA* dye starts to appear at 3669, 3131, and 1729 cm^{-1}. Results demonstrate no obvious difference

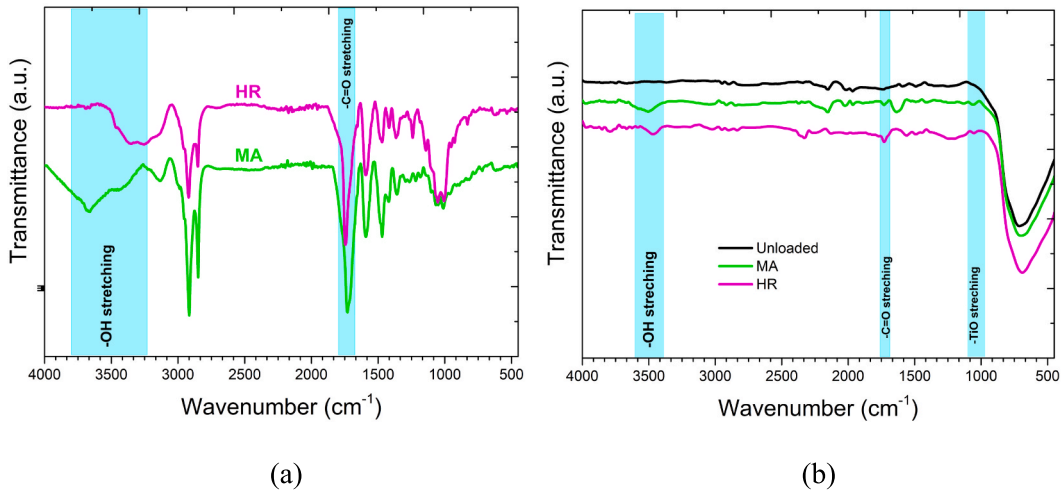

Fig. 1. (a) FT-IR spectra of natural dyes obtained from the *HR* and *MA* (b) The spectra of the photoanodes loaded and unloaded with dye.

vibration modes of the dyes probably due to their similar material composition. These results also suggest that chemical interactions between the dyes and TiO_2 might occur owing to the presence of aforementioned groups, facilitating to transfer of carriers to TiO_2 from the extracted pigments of the dyes.

Fig. 1b illustrates the spectra of the photoanodes loaded and unloaded with dye. The results release that the unloaded photoanode displays a low-intensity peak at 3335 cm^{-1}, while dye-loaded photoanodes display peaks, particularly near 3400 cm^{-1}. It is assumed that the presence of peaks revealing at approximately 1060 cm^{-1} is due to the stress vibrations resulting from interactions between titanium and oxygen. The presence of aforementioned peaks and their shifting in dye-loaded versus non-dye-loaded photoanodes clearly suggests that these dyes are successfully soaked onto surface and, therefore, suitable being sensitizers in photovoltaic devices [32–36].

UV–vis spectroscopy was used to ascertain the optical absorption properties of the dyes throughout a wavelength spectrum ranging from 200 to 800 nm (Fig. 2). The peaks in Fig. 2 appear 665 and 613 nm for *HR* and 664 nm for *MA* in the visible light range. The peaks in Fig. 2 emerged between 469 and 439 nm, and at 309 nm for *HR* dye suppose the availability of carotene and flavonoids compounds [37,38]. The peaks appeared at 419 and 443 nm of the *MA* correspond to anthocyanin compounds [39].

To better understand how the dyes influence the optical properties of photoanodes, we probe the dye-loaded and unloaded photoanodes UV–vis spectroscopy. Fig. 3 depicts the spectra of the photoanodes loaded and unloaded with dye. The inset of Fig. 3 shows cross sectional

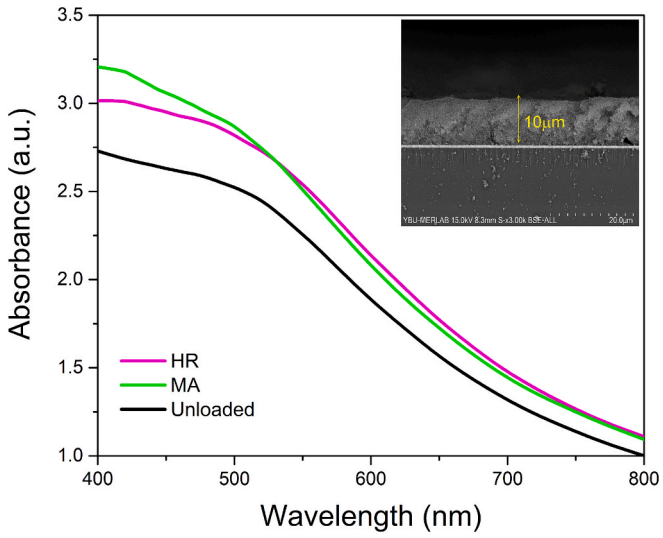

Fig. 3. UV–Vis spectra of the photoanodes loaded and unloaded with dye. Inset shows cross sectional view of the unloaded photoanode.

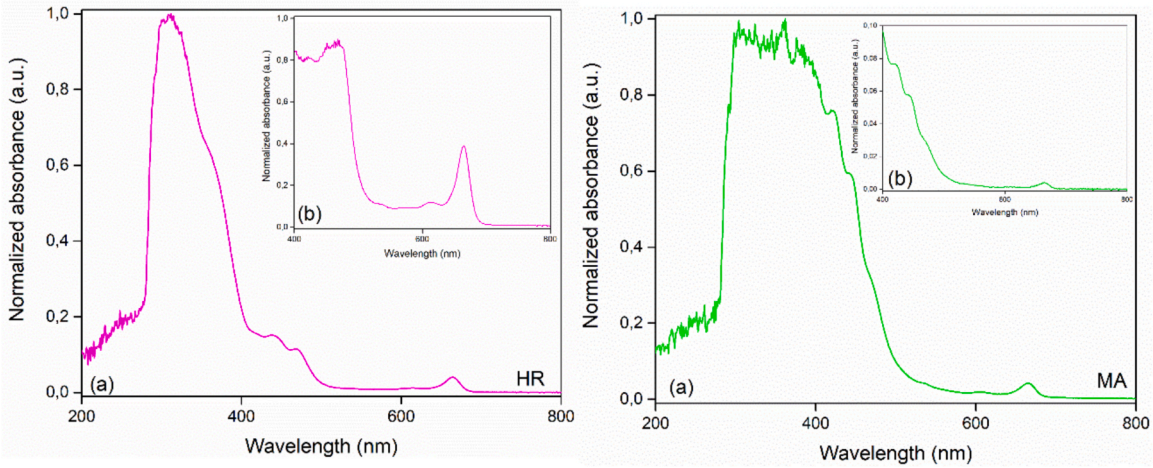

Fig. 2. UV–Vis spectra of the dyes: (a) dilute and (b) concentrate solutions.

view of the unloaded photoanode, revealing that photoanodes have 10 μm of thickness. The photoanode improved performance over the whole spectrum after dye loading, with the most significant improvement reported in the 400–600 nm range. It is apparent that the capacity for absorption of the *MA* loaded photoanode is better with respect to one loaded with *HR* is in the 400–530 nm range. In comparison, as for the *MA* loaded photoanode, we can still observe slightly higher absorbance above around 530 nm. These results further demonstrate that the incorporation of *HR* can improve optical properties of photoanodes to particularly benefit from longer wavelength of the light. To understand the electrochemical characteristics of the dyes and the electrolyte, we further attempt to have a deep insight into cyclic voltammetry (CV) studies (Fig. 4). The CV investigation was conducted with a CHI1020B electrochemical analyzer with a three-electrode cell configuration [40,41].

Fig. 4 displays *CV* plots for the dyes alongside the electrolyte (EL). Table 1 lists the parameters obtained from these graphs, where λ_{max} is absorption wavelength. The possibility for oxidation by ground (E_{OX}) was estimated as to be 0.466 and 0.479 V with respect to normal hydrogen electrode (NHE) for *HR* and *MA*, respectively. The optical band gap ($E_{0\text{-}0}$) was determined from their absorption onset and computed as 1.797 and 1.802 eV for *HR* and *MA*, respectively. The excited state oxidation potentials (E^*_{OX}) were found as −1.331 and −1.323 V with respect to NHE for *HR* and *MA*, respectively. The energy levels of the dyes were displayed in Fig. 5.

The level of HOMO for *HR* and *MA* is adequately positive relative to the energy level of EL (0.374 V *vs*. NHE), signifying that the EL functionally restores the dye which is oxidized. The CB of TiO_2 is significantly more negative with respect to LUMO of the dyes, proposing the possibility of injecting electrons into the CB of TiO_2 from the LUMO level [42,43].

To validate the findings from the characterizations of the dyes, NDSSCs consisting of an FTO/TiO_2/Dye/Pt/FTO structure was fabricated and their solar power output was evaluated under standard conditions. The current density–voltage (*J-V*) curve is displayed in Fig. 6. The inset of Fig. 6 shows pictures of the investigated plants and fabricated devices based on them. The parameters determined from Fig. 6 are summarized in Table 2 containing the average values based on five parallel measurements. Note that the obtained photovoltaic parameters show better values corresponding to the *HR*-based device, which, in terms of UV–Vis and CV characterizations, is mostly in line with the earlier findings.

Encouragingly, the *HR*-based device also possesses excellent optoelectronic properties, exhibiting 1.2 % of power conversion efficiency

Table 1
The parameters obtained from Fig. 4.

Dye	λ_{max} (nm)	E_{OX}/ E_{HOMO} (V)	$E_{0\text{-}0}$ (V)	E^*_{OX}/E_{LUMO} (V)	ΔG_{inj} (V)	ΔG_{reg} (V)
HR	665	0.466	1.797	−1.331	−0.831	−0.092
MA	664	0.479	1.802	−1.323	−0.823	−0.105

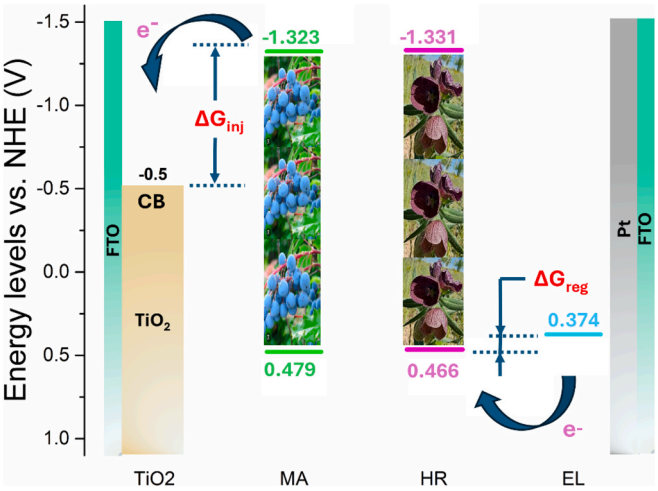

Fig. 5. Schematic energy level diagram of *HR*, and *MA* dyes as determined by cyclic voltammetry.

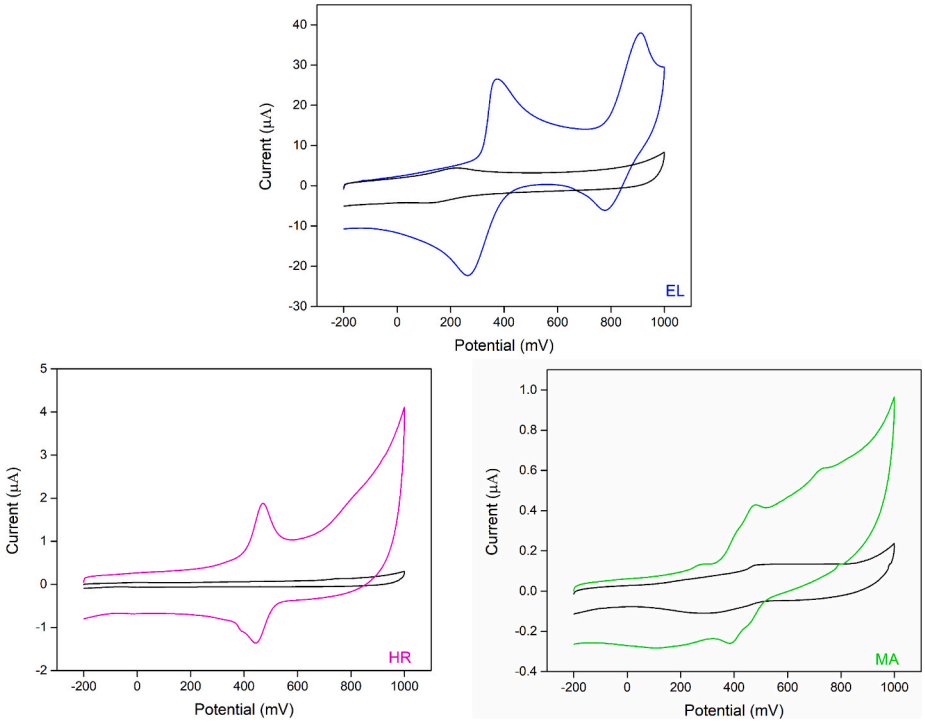

Fig. 4. *CV* plots for the *HR* dye, and *MA* dye together with the EL electrolyte.

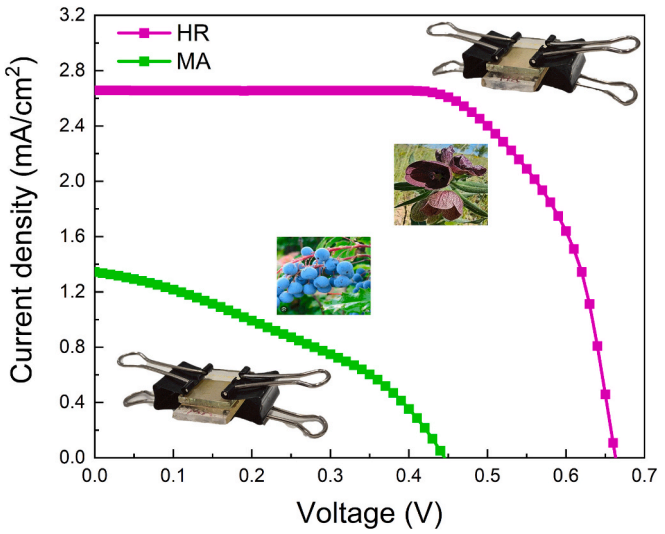

Fig. 6. Photocurrent voltage curves of DSSCs with *HR*, and *MA* sensitizers. The inset of Fig. 6 shows pictures of the investigated plants and fabricated devices based on them.

Table 2
Key photovoltaic properties of DSSCs utilizing various dyes.

Dye	J_{sc} (mA/cm^2)	V_{oc} (V)	*FF*	η (%)	R_{sh} (kΩ)	R_{se} (Ω)
HR	2.66	0.67	0.67	1.20	38.7	32.03
MA	1.34	0.45	0.37	0.22	0.75	120.72

(PCE) of with 2.66 mA/cm^2 of J_{sc}, 0.67 V of V_{oc} and 0.67 of *FF*, which outperforms *MA*-based device for all photovoltaics (0.22 % of PCE, 1.34 mA/cm^2 of J_{sc}, 0.45 V of V_{oc} and 0.37 of *FF*) measured the same conditions.

There is a lack of systematic studies based on experimentally determining driving forces in the natural DSSCs. An appropriate structure of natural dyes can lead to a LUMO located above *CB* of TiO_2, and concurrently a HOMO preferentially located close to the EL. Having such a design helps charge transfer and injection of electrons from the LUMO to *CB* of TiO_2, next, it is also beneficial for dye regeneration. The photovoltaic performance of the dyes demonstrates a direct correlation between the efficiency and the driving forces of electron injection and dye regeneration [44,45]. So, to more accurately elucidate our results, underlying forces and interfacial resistance values were calculated, which significantly affect power conversion efficiency, J_{sc}, V_{oc} and *FF* values in NDSSCs. If injection originates from dye which is exciting, underlying force for injection (ΔG_{inj}) is represented by the following formula upon photoexcitation [46]

$$\Delta G_{inj} = E_{OX}^{dye^*} - E_{CB}^{SC} \quad (1)$$

where $E_{OX}^{dye^*}$ and E_{CB}^{SC} are oxidation potential of the excited-state and the edge of CB of TiO_2, respectively. $E_{OX}^{dye^*}$ can be estimated from the following:

$$E_{OX}^{dye^*} = E_{OX}^{dye} - E_{0-0} \quad (2)$$

where E_{OX}^{dye} and E_{0-0} denote the ground-state oxidation potential and energy corresponding to the maximum absorption, respectively.

The difference in energy between the potential of redox ($E_{redox}^{electrolyte}$) and E_{OX}^{dye} determines a driving force for dye regeneration (ΔG_{reg}) [47]:

$$\Delta G_{reg} = E_{redox}^{electrolyte} - E_{OX}^{dye} \quad (3)$$

To get additional understanding of the impact of forces, ΔG_{inj} and ΔG_{reg} of each dye were computed, and compiled in Table 1. Note that our values match those described in the literature quite well [44,45]. $E_{OX}^{dye^*}$ values are more negative for both dyes than those of CB of TiO_2, suggesting efficient injection of electrons. The dyes have high absolute values of ΔG_{inj}, which is relatively higher for *HR* compared to *MA*. This demonstrates that *HR* is more effectively injecting electrons into TiO_2. Since *HR* has superior optical properties and sufficient injection driving force when compared to *MA*, one can easily conclude that the device consisting of *HR* has a higher J_{sc} [48,49].

Avoiding charge recombination and promoting undesired charge transfer are two advantages of efficient dye regeneration. The ΔG_{reg} of *HR* is lower than that of *MA*, as shown in Table 1. It unveils that the coexistence of *HR* and electrolyte employed may encourage the regeneration of oxidized dyes. Therefore, one can expect that the device consisting of *HR* has a higher V_{oc} with respect to *MA* [48,50].

In addition, the superior overall efficiency for *HR* may be also attributed to its elevated *FF* value. The resistance, which includes shunt (R_{sh}) and series resistance (R_{se}) have a strong correlation with the *FF* [3]. Recent research has significantly advanced our understanding of charge transport mechanisms in thin-film semiconductor materials for optoelectronic devices. Studies on modified TiO_2 systems reveal distinct conduction behaviors – Fe-doped amorphous films demonstrate multiphonon-assisted hopping conduction above 391 K [51], while undoped TiO_2 follows variable-range hopping mechanisms at lower temperatures [52]. Similar investigations in ZnO systems show that optimal aluminum doping (3 wt%) enhances conductivity by modifying trap states and grain boundary effects [53]. The temperature-dependent localization effects [54,55] and leakage current [56] should also be considered in carrier transport, enabling remarkable device innovations. In photovoltaics, plasmonic core–shell nanostructures boost dye-sensitized solar cell efficiency to 7.41 % through enhanced light-matter interactions [57], while optimized TiO_2 processing techniques improve electron lifetimes for significantly better device performance [58]. Together, these findings demonstrate how careful material design and processing control can affect charge transport mechanisms. Ultimately, appropriate values of resistance should be obtained for better carrier transport. It is certain that a cell with low R_{se} and high R_{sh} has a high *FF* and thus lead to a higher conversion efficiency [3]. Those resistance were extracted from the slope of *J-V* curve and listed in Table 2. In our case, it is observed that the *HR*-based device has a low value of R_{se} but high value of R_{sh} compared to *MA* based device, leading to an improvement in *FF*.

To comprehend a correlation between interfacial resistance dynamics and the photovoltaic properties of the devices, EIS measurements were provided. The measurements were conducted in dark conditions with a bias voltage approximately matching V_{oc}. Figs. 7 and 8 represent the Nyquist and the Bode plots of the devices, respectively. The inset of Fig. 7 displays the used appropriate equivalent circuit model to fit EIS parameters [13,15]. The fitted EIS variables, including the FTO's resistance (R_s), charge transfer resistance (R_{ct}), recombination resistance (R_{rec}), electron lifetime (τ) and the charge collection efficiency (η_{cc}) are summarized in Table 3. The Nyquist plots are composed of two semicircles. The left semicircle at higher frequency related to the charge transfer resistance (R_{ct}) at the interface of Pt/electrolyte and the right semicircle at lower frequency correspond to the recombination resistance (R_{rec}) [58,59].

It is evident that the charge transfer resistance (R_{ct}) and series resistance (R_s) values are very close to each other verifying the fact that both devices were fabricated under the same conditions. On the other hand, since the value of R_{rec} of *HR*-based cell is remarkably higher than that of *MA*-based cell, this case can greatly affect its V_{oc} value [58,59], which is consistent of our *J-V* results. Regarding the charge collection efficiency of the devices, we can consider the equation of $\eta_{cc} = [1 + (R_{ct}/R_{rec})]^{-1}$ [60], confirming evidence of how quickly electron transport

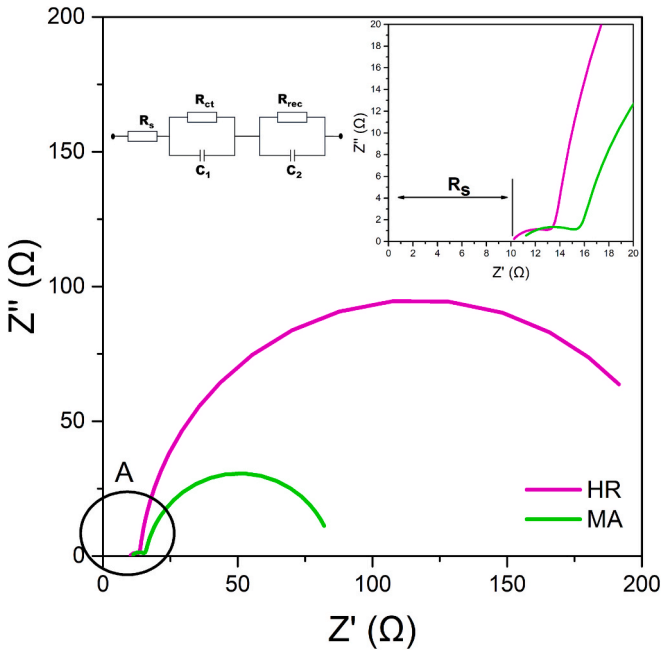

Fig. 7. Nyquist diagrams of the cells utilizing the analyzed dyes.

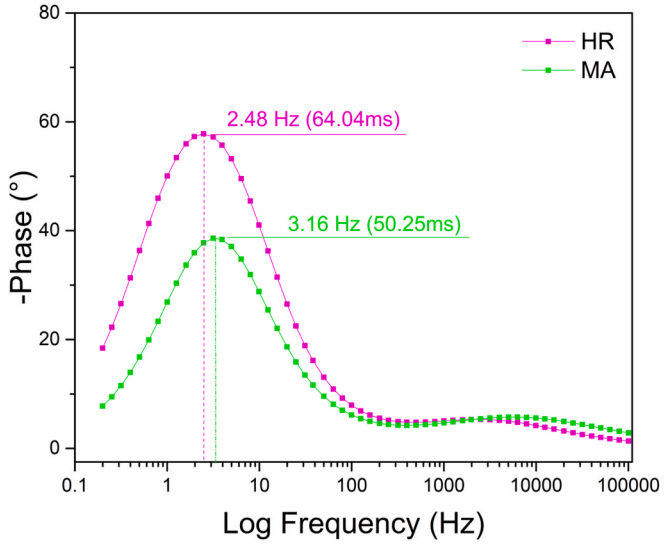

Fig. 8. Bode plot of the cells based on the investigated dyes.

Table 3
Estimated fitting parameters based on EIS measurements of the *HR and MA* natural dye based DSSCs.

Dye	R_s (Ω)	R_{rec} (Ω)	R_{ct} (Ω)	τ (ms)	η_{cc} (%)
HR	3.61	207	9.95	64.04	95.4
MA	5.3	69.48	10.69	50.25	86.7

occurs. It is predicted that a relatively higher value of η_{cc} of the *HR*-based device possesses better charge transfer, boosting the overall performance of the device.

To make our conclusions more convincing, we further consider Bode graph (Fig. 8) to probe the lifetime which is a key parameter indicating the performance. By using $\tau = 1/(2\pi f_{max})$, one can estimate the lifetime. The electron lifetime can be estimated through [58,59], where f_{max} the peaks in the low-frequency section of the plots are illustrated in Fig. 8 and listed in Table 3. The *HR*-based cell has longer electron lifetime than that of *MA*-based cell, which verifies decreased rate of recombination and better V_{oc} [58,59]. The trend in the electron lifetime is in line with the V_{oc} of the devices.

4. Conclusions

We have successfully developed *Hyoscyamus reticulatus* and *Mahonia aquifolium* dyes based-DSSCs. To understand the mechanisms and overall photovoltaic characteristics of illuminated solar cells, *C-V*, *J-V*, and EIS measurements were conducted. The short-circuit current was improved because of a greater driving force associated with injection, whereas open-circuit voltage demonstrated an enhancement in a small driving force associated with regeneration. Based on our outcomes, among the tested natural DSSCs under similar conditions, *HR* exhibited superior output value for an efficiency of 1.20 %. Our study on NDSSCs paves the way for further research exploring the importance of underlying forces behind electron injection and dye regeneration in such photovoltaic devices.

CRediT authorship contribution statement

M.E. Yelkovan: Writing – original draft, Visualization, Methodology, Data curation. **M. Erdogdu:** Writing – original draft, Supervision. **Y. Erdogdu:** Writing – original draft, Supervision. **A. Yildiz:** Writing – original draft, Supervision, Investigation.

Declaration of competing interest

The authors declare that they have no known competing financial interests or personal relationships that could have appeared to influence the work reported in this paper.

Acknowledgments

The authors thank the Gazi University Research Fund (Project Number: FGA-2023-9011) for its financial support. This work is based on the doctoral work of Enes Yelkovan.

References

[1] R.N. Iman, et al., A comprehensive review on advancements and optimization strategies in dye-sensitized solar cells: Components, characterization, stability and efficiency enhancement, Inorg. Chem. Commun. 165 (2024) 112488, https://doi.org/10.1016/j.inoche.2024.112488.
[2] A. Atli, A. Yildiz, Opaque Pt counter electrodes for dye-sensitized solar cells, Int. J. Energy Res. 46 (2022) 6543–6552, https://doi.org/10.1002/er.7590.
[3] C. Altinkaya, A. Atli, A. Atilgan, K. Salimi, A. Yildiz, Facile fabrication of low-cost low-temperature carbon-based counter electrode with an outstanding fill factor of 73% for dye-sensitized solar cells, Int. J. Energy Res. 44 (2020) 3160–3170, https://doi.org/10.1002/er.5174.
[4] A.F. Abdelaal, et al., Fabrication of efficient and economical dye-sensitized solar cells using carbon-coated nanotextured silicon wafers counter electrodes, Synthetic Metals 301 (2024) 117537, https://doi.org/10.1016/j.synthmet.2023.117537.
[5] A. Atilgan, A. Yildiz, Ni-doped TiO 2 / TiO 2 homojunction photoanodes for efficient dye-sensitized solar cells, Int. J. Energy Res. 46 (2022) 14558–14569, https://doi.org/10.1002/er.8175.
[6] A. Atli, A. Yildiz, Hybrid TiO2 nanorods combined with a buffer layer for dye-sensitized solar cells, Appl. Solar Energy 58 (2022) 323–329, https://doi.org/10.3103/s0003701x22030045.
[7] K. Ozel, A. Atilgan, A. Yildiz, Multi-layered blocking layers for dye sensitized solar cells. Journal of Photochemistry and Photobiology a, Chemistry 448 (2023) 115297, https://doi.org/10.1016/j.jphotochem.2023.115297.
[8] A. Razaghizadeh, V. Rafee, R. Nakhaei, Effect of silver nanoparticles embedding in mesoporous TiO2 layer on the performance enhancement of dye-sensitized solar cells using natural dyes, Plasmonics (2025) 1–15. https://link.springer.com/article/10.1007/s11468-025-02836-5.
[9] K. Inbarajan, et al., Soxhlet extraction of natural dyes from the husk of Cocos nucifera and their efficacious application as sensitizer in TiO2 based dye sensitized solar cells, Opt. Quant. Electron. 57 (1) (2025) 1–17. https://link.springer.com/article/10.1007/s11082-024-07963-7.

[10] N. Al-Shamery, et al., From black pigment to green energy: shedding light on melanin electrochemistry in dye-sensitized solar cells, Mater. Adv. (2025) https://pubs.rsc.org/en/content/articlehtml/2025/ma/d5ma00081e.

[11] Haoran Zhou, et al., Key materials and fabrication strategies for high-performance dye-sensitized solar cells: comprehensive comparison and perspective, ACS Energy Lett. 10 (2025) 881–895, https://pubs.acs.org/doi/abs/10.1021/acsenergylett.4c03579.

[12] Y. Kocak, A. Atli, A. Atilgan, A. Yildiz, Extraction method dependent performance of bio-based dye-sensitized solar cells (DSSCs), Mater. Res. Express 6 (2019) 095512, https://doi.org/10.1088/2053-1591/ab2ef7.

[13] M. Erdoğdu, A. Atilgan, Y. Erdogdu, A. Yildiz, Natural dyes extracted from Ligustrum vulgare, Juniperus sabina, and Papaver rhoeas for novel DSSC applications, Mater. Lett. 358 (2023) 135811, https://doi.org/10.1016/j.matlet.2023.135811.

[14] Y. Kocak, A. Yildiz, Carminic acid extracted from cochineal insect as photosensitizer for dye-sensitized solar cells, Int. J. Energy Res. 45 (2021) 16901–16907, https://doi.org/10.1002/er.6883.

[15] M. Erdogdu, A. Atilgan, Y. Erdogdu, A. Yildiz, Flavonoid from Hedera helix fruits: A promising new natural sensitizer for DSSCs, J. Photochem. Photobiol. Chem. 448 (2023) 115288, https://doi.org/10.1016/j.jphotochem.2023.115288.

[16] N. Akdogan, M. Alp, A. Atilgan, A. Disli, Y. Erdogdu, A. Yildiz, An AZO dye with nitril anchoring to dye-sensitized solar cell performance: A theoretical and experimental investigation, Mater. Lett. 351 (2023) 135075, https://doi.org/10.1016/j.matlet.2023.135075.

[17] N. Akdogan, B. Ortatepe, A. Atli, A. Disli, Y. Erdogdu, A. Yildiz, A joint theoretical and experimental study on a Tetrazole-Anchored BODIPY-Based dye at the surface of TIO2 for Dye-Sensitized solar cell applications, Physica Status Solidi (a). 221 (2023), https://doi.org/10.1002/pssa.202300513.

[18] R.N. Iman, K. Harrabi, M. Younas, A. Mekki, Fabrication of efficient natural dye-sensitized Solar Cells using Mediterranean olive leaves as natural dye sensitizer, J. Photochem. Photobiol. Chem. 450 (2024) 115477, https://doi.org/10.1016/j.jphotochem.2024.115477.

[19] R.N. Iman, M. Younas, K. Harrabi, A. Mekki, Fabrication and characterization of natural dye-sensitized solar cells using an efficient natural sensitizer derived from Laurus nobilis L, Dyes Pigm. 225 (2024) 112057, https://doi.org/10.1016/j.dyepig.2024.112057.

[20] A. Mahapatra, P. Kumar, A.K. Behera, A. Sen, B. Pradhan, Comparative study of natural dye-sensitized solar cells using inedible extracts from kumkum, kamala and malabar spinach fruits. Journal of Photochemistry and Photobiology a, Chemistry 436 (2022) 114385, https://doi.org/10.1016/j.jphotochem.2022.114385.

[21] T. Rajaramanan, F.H. Gourji, Y. Elilan, S. Yohi, M. Senthilnanthanan, P. Ravirajan, D. Velauthapillai, Natural sensitizer extracted from Mussaenda erythrophylla for dye-sensitized solar cell, Sci. Rep. 13 (2023), https://doi.org/10.1038/s41598-023-40437-6.

[22] Z. Yousaf, S. Masood, Z.K. Shinwari, M.A. Khan, A. Rabani, Evaluation of taxonomic status of medicinal species of the genus *Hyoscyamus, Withania, Atropa* and *Datura* based on polyacrylamide gelelectrophoresis, Pak. J. Bot. 40 (6) (2008) 2289–2297.

[23] K.B. Supria, Handbook of Medicinal Plants, Poiter Publishers, India, 1998, p. 607.

[24] T. Baytop, Türkiye'de Bitkilerle Tedavi, 2.baskı, Nobel Tıp Kitabevleri (1999).

[25] D. Minore, P.O. Rudolf, F.T. ve Bonner, Mahonia nutt. Oregon-grape, in: The Woody Plant Seed Manual, 2008, pp. 706–710.

[26] Mamıkoğlu, N.G. 2017. Turkiye'nin Ağacları ve Calıları. 7. Basım, Kırmızı Kedi Yayınevi, İstanbul.

[27] H. Coklar, M. Akbulut, Anthocyanins and phenolic compounds of Mahonia aquifolium berries and their contributions to antioxidant activity, J. Funct. Foods 35 (2017) 166–174, https://doi.org/10.1016/j.jff.2017.05.037.

[28] P. Akbaş, H. Uslu, G.A. Uslu, H. Alkan, Hyoscyamus reticulatus L. Tohum Ekstraktının Antimikrobiyal ve Apoptotik Etkinliğinin Araştırılması, Süleyman Demirel Üniversitesi Fen Bilimleri Enstitüsü Dergisi. 24 (2020) 317–322. https://doi.org/10.19113/sdufenbed.631074.

[29] A.E. Al-Snafi, Therapeutic importance of Hyoscyamus species grown in Iraq (Hyoscyamus albus, Hyoscyamus niger and Hyoscyamus reticulates)-A review, IOSR J. Pharm. 8 (6) (2018) 18–32.

[30] Y. Erdogdu, Investigations of FT-IR, FT-Raman, FT-NMR spectra and quantum chemical computations of Esculetin molecule, Spectrochim. Acta A Mol. Biomol. Spectrosc. 106 (2012) 25–33, https://doi.org/10.1016/j.saa.2012.12.043.

[31] Y. Erdogdu, U.C. Baskose, S. Saglam, M. Erdogdu, H. Ogutcu, S. Özçelik, Structural, thermal, spectroscopic, electronic and biological activity properties of coumarin-153 dyes for DSSCs: A DFT benchmark study, J. Mol. Struct. 1221 (2020) 128873, https://doi.org/10.1016/j.molstruc.2020.128873.

[32] V. Yadav, C.M.S. Negi, D.K. Kumar, S.K. Gupta, Fabrication of eco-friendly, low-cost dye sensitized solar cells using harda fruit-based natural dye, Opt. Mater. 122 (2021) 111800, https://doi.org/10.1016/j.optmat.2021.111800.

[33] F.M.M.D. Santos, A.M.B. Leite, L.R.B. Da Conceição, Y. Sasikumar, R. Atchudan, M. F. Pinto, R.S. Babu, A.L.F. De Barros, Effect of bandgap energies by various color petals of Gerbera jamesonii flower dyes as a photosensitizer on enhancing the efficiency of dye-sensitized solar cells, J. Mater. Sci. Mater. Electron. 33 (2022) 20338–20352, https://doi.org/10.1007/s10854-022-08849-8.

[34] L.R.B. Da Conceicao, A.L.F. De Barros, D.B. Haddad, R.S. Babu, Passiflora edulis and Cocos nucifera extracts as light-harvesters for efficient dye-sensitized solar cells, IEEE ANDESCON 1–5 (2020), https://doi.org/10.1109/andescon50619.2020.9272107.

[35] S. Jeyaram, T. Geethakrishnan, Vibrational spectroscopic, linear and nonlinear optical characteristics of Anthocyanin extracted from blueberry, Results Opt. 1 (2020) 100010, https://doi.org/10.1016/j.rio.2020.100010.

[36] F.C. Ferreira, R.S. Babu, A.L.F. De Barros, S. Raja, L.R.B. Da Conceição, L.H. C. Mattoso, Photoelectric performance evaluation of DSSCs using the dye extracted from different color petals of Leucanthemum vulgare flowers as novel sensitizers, Spectrochim. Acta Part A Mol. Biomol. Spectrosc. 233 (2020) 118198, https://doi.org/10.1016/j.saa.2020.118198.

[37] Bechtold, T., Mussak, R.: Handbook of Natural Colorants. (2009). https://doi.org/10.1002/9780470744970.

[38] W.O.N.S. Halidun, E.C. Prima, B. Yuliarto, N. Suyatman, Fabrication dye sensitized solar cells (DSSCs) using B-Carotene pigment based natural dye, MATEC Web Conf. 159 (2018) 02052, https://doi.org/10.1051/matecconf/201815902052.

[39] S. Saha, J. Singh, A. Paul, R. Sarkar, Z. Khan, K. Banerjee, Anthocyanin profiling using UV-VIS spectroscopy and liquid chromatography mass spectrometry, J. AOAC Int. 103 (2019) 23–39, https://doi.org/10.5740/jaoacint.19-0201.

[40] S. Donmez, F. Arslan, H. Arslan, A nucleic acid biosensor for detection of hepatitis C virus genotype 1A using Poly(L-Glutamic Acid)-Modified electrode, Appl. Biochem. Biotechnol. 176 (2015) 1431–1444, https://doi.org/10.1007/s12010-015-1655-6.

[41] S. Donmez, L. Çağdaş, H. Arslan, F. Arslan, Electrochemical nucleic acid hybridization biosensor based on poly(L-Aspartic acid)-modified electrode for the detection of short oligonucleotide sequences related to hepatitis C virus 1a, Prep. Biochem. Biotech. 49 (2019) 900–907, https://doi.org/10.1080/10826068.2019.1636279.

[42] W. Ying, F. Guo, J. Li, Q. Zhang, W. Wu, H. Tian, J. Hua, Series of new D-A-Π-A organic broadly absorbing sensitizers containing iSoindigo unit for highly efficient dye-sensitized solar cells, ACS Appl. Mater. Interfaces 4 (2012) 4215–4224, https://doi.org/10.1021/am300925e.

[43] Z. She, Y. Cheng, L. Zhang, X. Li, D. Wu, Q. Guo, J. Lan, R. Wang, J. You, Novel ruthenium sensitizers with a phenothiazine conjugated bipyridyl ligand for high-efficiency dye-sensitized solar cells, ACS Appl. Mater. Interfaces 7 (2015) 27831–27837, https://doi.org/10.1021/acsami.5b09160.

[44] S. Akın, S. Açıkgöz, M. Gülen, C. Akyürek, S. Sönmezoğlu, Investigation of the photoinduced electron injection processes for natural dye-sensitized solar cells: the impact of anchoring groups, RSC Adv. 6 (2016) 85125–85134, https://doi.org/10.1039/c6ra19653e.

[45] S.H. Aung, Y. Hao, T.Z. Oo, G. Boschloo, Kinetic study of carminic acid and santalin natural dyes in dye-sensitized solar cells, J. Photochem. Photobiol. A Chem. 325 (2016) 1–8, https://doi.org/10.1016/j.jphotochem.2016.03.022.

[46] J. Preat, C. Michaux, D. Jacquemin, E.A. Perpète, Enhanced efficiency of organic Dye-Sensitized solar cells: triphenylamine derivatives, J. Phys. Chem. C 113 (2009) 16821–16833, https://doi.org/10.1021/jp904946a.

[47] M. Li, L. Kou, L. Diao, Q. Zhang, Z. Li, Q. Wu, W. Lu, D. Pan, Z. Wei, Theoretical study of WS-9-Based organic sensitizers for unusual VIS/NIR absorption and highly efficient Dye-Sensitized solar cells, J. Phys. Chem. C 119 (2015) 9782–9790, https://doi.org/10.1021/acs.jpcc.5b03667.

[48] Z. Zhang, W. Hu, R. He, W. Shen, M. Li, The influence of inserted thiophene into the (π-A'-π)-bridge on photovoltaic performances of dye-sensitized solar cells, Mater. Chem. Phys. 191 (2017) 121–128, https://doi.org/10.1016/j.matchemphys.2017.01.042.

[49] K.S. Dhivya, C. Senthilkumar, K. Karthika, P. Srinivasan, Theoretical, structural, and electronic analyses of pyridin-based dyes for dye-sensitized solar cells applications, J. Mol. Model. 30 (2024), https://doi.org/10.1007/s00894-024-06002-2.

[50] Y. Xie, J. Baillargeon, T.W. Hamann, Kinetics of regeneration and recombination reactions in Dye-Sensitized solar cells employing Cobalt redox shuttles, J. Phys. Chem. C 119 (2015) 28155–28166, https://doi.org/10.1021/acs.jpcc.5b08244.

[51] D. Mardare, A. Yildiz, R. Apetrei, P. Rambu, D. Florea, N.G. Gheorghe, D. Macovei, C.M. Teodorescu, D. Luca, The Meyer–Neldel rule in amorphous TiO2 films with different Fe content, J. Mater. Res. 27 (2012) 2271–2277, https://doi.org/10.1557/jmr.2012.193.

[52] A. Yildiz, S. Lisesivdin, M. Kasap, D. Mardare, High temperature variable-range hopping conductivity in undoped TiO2 thin film, Optoelectron. Adv. Mater.-Rapid Commun. 1 (2007) 531–533.

[53] T. Serin, A. Atilgan, I. Kara, A. Yildiz, Electron transport in Al-Cu co-doped ZnO thin films, J. Appl. Phys. 121 (2017), https://doi.org/10.1063/1.4977470.

[54] S.B. Lisesivdin, A. Yildiz, S. Acar, M. Kasap, S. Ozcelik, E. Ozbay, Electronic transport characterization of AlGaN/GaN heterostructures using quantitative mobility spectrum analysis, Appl. Phys. Lett. 91 (2007), https://doi.org/10.1063/1.2778453.

[55] S.B. Lisesivdin, N. Balkan, O. Makarovsky, A. Patanè, A. Yildiz, M.D. Caliskan, M. Kasap, S. Ozcelik, E. Ozbay, Large zero-field spin splitting in AlGaN/AlN/GaN/AlN heterostructures, J. Appl. Phys. 105 (2009), https://doi.org/10.1063/1.3120782.

[56] K. Ozel, A. Yildiz, A self-powered ultraviolet photodetector with ultrahigh photoresponsivity (208 mA W−1) based on SnO2 nanostructures/Si Heterojunctions, Phys. Status Solidi (RRL) - Rapid Res. Lett. 15 (2021), https://doi.org/10.1002/pssr.202100085.

[57] K. Salimi, A. Atilgan, M.Y. Aydin, H. Yildirim, N. Celebi, A. Yildiz, Plasmonic mesoporous core-shell Ag-Au@TiO2 photoanodes for efficient light harvesting in dye sensitized solar cells, Sol. Energy 193 (2019) 820–827, https://doi.org/10.1016/j.solener.2019.10.039.

[58] A. Atli, I. Sutcu, Z.K. Yildiz, A. Yildiz, Optimizing deposition parameters of DSSCs composed of blue TIO2, IEEE J. Photovolt. 11 (2020) 118–123, https://doi.org/10.1109/jphotov.2020.3038602.
[59] J.-S. Ni, T.-Y. Chiu, W.-S. Kao, H.-J. Chou, C.-C. Su, J.T. Lin, Organic photosensitizers incorporating rigidified dithieno[3,2-f:2′,3′-h]quinoxaline segment tethered with thiophene substitutes for dye-sensitized solar cells, ACS Appl. Mater. Interfaces 8 (2016) 23066–23073, https://doi.org/10.1021/acsami.6b07346.
[60] X. Zhang, J. Mao, D. Wang, X. Li, J. Yang, Z. Shen, W. Wu, J. Li, H. Ågren, J. Hua, Comparative study on Pyrido[3,4-b]pyrazine-based sensitizers by tuning bulky donors for dye-sensitized solar cells, ACS Appl. Mater. Interfaces 7 (2015) 2760–2771, https://doi.org/10.1021/am507824h.